

MIT Open Access Articles

Metal-Organic Framework-Derived Guerbet Catalyst Effectively Differentiates between Ethanol and Butanol

The MIT Faculty has made this article openly available. **Please share** how this access benefits you. Your story matters.

Citation: Neumann, Constanze et al. "Metal-Organic Framework-Derived Guerbet Catalyst Effectively Differentiates between Ethanol and Butanol." *Journal of the American Chemical Society* 141, 44 (October 2019): 17477-17481 © 2019 American Chemical Society.

As Published: <http://dx.doi.org/10.1021/jacs.9b08968>

Publisher: American Chemical Society (ACS)

Persistent URL: <https://hdl.handle.net/1721.1/124650>

Version: Author's final manuscript: final author's manuscript post peer review, without publisher's formatting or copy editing

Terms of Use: Article is made available in accordance with the publisher's policy and may be subject to US copyright law. Please refer to the publisher's site for terms of use.



Metal–Organic Framework-Derived Guerbet Catalyst Effectively Differentiates between Ethanol and Butanol

Constanze N. Neumann,[†] Steven J. Rozeveld,[‡] Mingzhe Yu,[‡] Adam J. Rieth,[†] and Mircea Dincă^{*,†}

[†]Department of Chemistry, Massachusetts Institute of Technology, 77 Massachusetts Avenue, Cambridge, Massachusetts 02139, United States

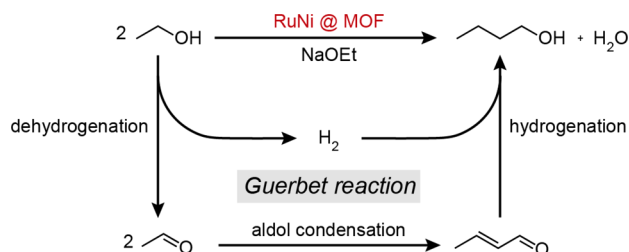
[‡]Core R&D, The Dow Chemical Company, Midland, Michigan 48674, United States

S Supporting Information

ABSTRACT: RuNi nanoparticles supported on a metal–organic framework (RuNi@MOF) and formed in situ from a ruthenium complex enclosed inside a nickel-based MOF act as a highly active catalyst for the Guerbet reaction of ethanol to 1-butanol, providing turnover numbers up to 725 000 Ru^{−1}. Negligible activity of the RuNi@MOF ethanol upgrading catalyst system toward chemically similar 1-butanol makes it possible to synthesize the competent Guerbet substrate 1-butanol with >99% selectivity.

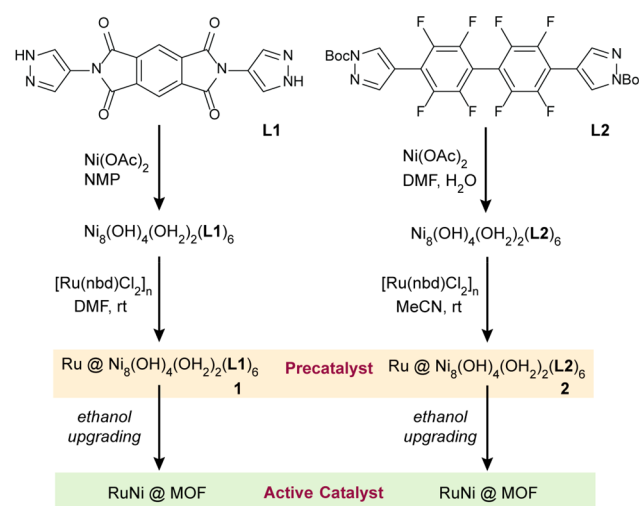
Achieving high selectivity for a desired product in a catalytic reaction is exceedingly challenging when the

Scheme 1. Proposed Mechanism of EtOH Upgrading to *n*-BuOH



starting material and the product bear strong chemical resemblance, because the product itself can act as a substrate, leading to oligomerization and polymerization. Indeed, polymerization reactions rely on the fact that the catalyst continues to add monomers to a growing chain because the same functional group terminates the polymer after every addition of monomer.¹ The synthesis of 1-butanol (*n*-BuOH) from ethanol (EtOH) via the Guerbet reaction, on the other hand, is an example of a reaction where the ideal catalyst would display very high activity for the conversion of EtOH, but be unreactive toward *n*-BuOH, which only differs from EtOH by the length of the primary alcohol's carbon chain. Beyond the academic interest in achieving differential catalytic selectivity toward chemically similar compounds, the efficient conversion of EtOH to *n*-BuOH is desirable because *n*-BuOH is a promising drop-in alternative to gasoline.^{2,3} Although EtOH itself can replace a fraction of gasoline in transportation fuel, EtOH, unlike *n*-BuOH, cannot

Scheme 2. Synthetic Scheme for Accessing MOF-Derived Guerbet Pre-catalysts for EtOH Upgrading to *n*-BuOH



be transported via pipelines or fully replace gasoline for use in cars without special engine modifications.^{2–4} Due to its considerably lower corrosiveness, as well as physical and chemical properties that more closely resemble gasoline, *n*-BuOH can serve as a drop-in biofuel if obtained from a renewable source such as bio-derived EtOH.^{4,5}

The homogeneous and heterogeneous catalysts currently available for the Guerbet upgrading of EtOH to *n*-BuOH show distinct side product profiles: whereas homogeneous Guerbet catalysts commonly produce sodium acetate and C₆₊ alcohols as undesirable side products, heterogeneous catalysts tend to form undesirable olefins, ethers, alkanes, as well as C₆₊ alcohols.^{6–23} Furthermore, although homogeneous Guerbet reactions can be conducted at 150–160 °C, heterogeneous Guerbet reactions typically require temperatures in excess of 250 °C for practical reaction rates. A more desirable catalyst is one that combines the process advantages of heterogeneous catalysts, but operates below 200 °C and produces minimal side products.

One class of compounds that share characteristics of both homogeneous and heterogeneous catalysts and are therefore well positioned to answer this challenge is metal–organic

Received: August 19, 2019

Published: October 22, 2019

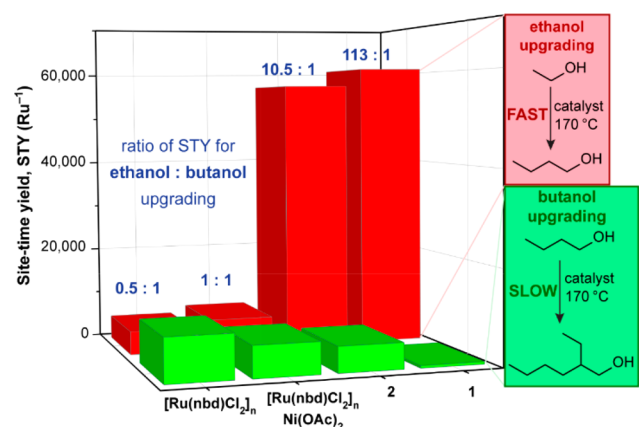


Figure 1. Comparison of site-time yield (STY) for *n*-BuOH production (red bars) and 2-ethyl-hexanol production (green bars) in the Guerbet upgrading of neat EtOH (containing 21 wt% NaOEt) and neat *n*-BuOH (containing 21 wt% NaOBu), respectively, with 1, 2, and control Ru and Ru/Ni systems after 14.5 h at 170 °C.

frameworks (MOFs). We thus set out to develop new MOF-based Guerbet catalysts, focusing in particular on the design of a catalyst that can effectively differentiate between the chemically similar EtOH starting material and the *n*-BuOH product, and can thus prevent the formation of higher alcohol products.^{24–26}

Inspired by highly active ruthenium-based homogeneous catalysts for EtOH upgrading,^{9,13,15,16} we incorporated simple ruthenium compounds into the pore space of MOFs featuring different secondary building units (SBUs) and topologies. To our surprise, the reductive reaction conditions of the Guerbet reaction did not simply induce reduction of pore-confined ruthenium precursors to form Ru nanoparticles, but also led to the reduction of a small fraction of the first-row transition metal comprising the MOF SBU to yield alloyed Ru nanoparticles. This presented the possibility of limiting the use of precious metal by alloying with a cheaper first-row transition metal.

Most notable was an increased activity observed when nickel was added to EtOH upgrading catalyzed by commercially available $[\text{Ru}(\text{nbd})\text{Cl}_2]_n$ (nbd = norbornadiene; Table S1). We thus sought to identify a nickel-based MOF that would be stable to water, polar organic solvents, base,

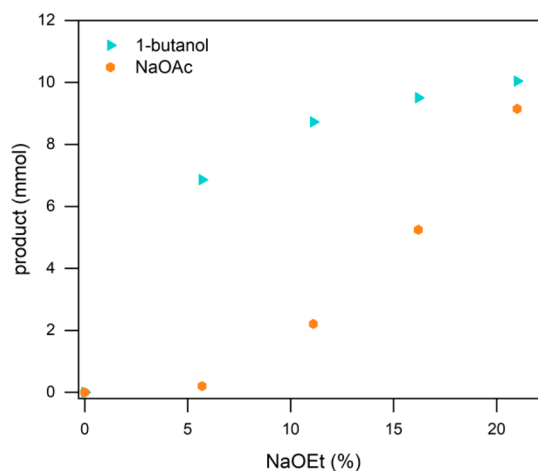


Figure 2. Formation of undesirable NaOAc can be virtually eliminated by decreasing the NaOEt content. Results are shown for reactions with 2 after 14.5 h at 170 °C.

and high reaction temperatures, the typical conditions for the Guerbet reaction. To this end, we selected water-stable $\text{Ni}_8(\text{OH})_4(\text{OH}_2)_2(\text{L1})_6$ (L1 = 2,6-bis(1*H*-pyrazol-4-yl)-pyrrolo[3,4-*f*]isoindole-1,3,5,7(2*H*,6*H*)-tetrone, Figure S1) as a promising starting point.²⁷ Furthermore, given the formation and destruction of charged and/or highly polar intermediates in the proposed catalytic cycle (Scheme 1) we considered that the polarity of the pore environment could be crucial to catalysis. To evaluate the importance of pore polarity, we also targeted a new MOF, $\text{Ni}_8(\text{OH})_4(\text{OH}_2)_2(\text{L2})_6$ (L2 = 4,4'-(perfluoro-[1,1'-biphenyl]-4,4'-diyl)bis(1*H*-pyrazole), which is isostructural to $\text{Ni}_8(\text{OH})_4(\text{OH}_2)_2(\text{L1})_6$, but significantly more hydrophobic (Figures S2–S4). A convenient strategy to incorporate ruthenium into $\text{Ni}_8(\text{OH})_4(\text{OH}_2)_2(\text{L1})_6$ and $\text{Ni}_8(\text{OH})_4(\text{OH}_2)_2(\text{L2})_6$ is to soak the as-synthesized MOFs in a suspension of ruthenium(II) precursor $[\text{Ru}(\text{nbd})\text{Cl}_2]_n$ in a polar solvent (Scheme 2, Figure S5). This produces $\text{Ru}@$ MOF pre-catalysts 1 ($\text{Ru}@$ $\text{Ni}_8(\text{OH})_4(\text{OH}_2)_2(\text{L1})_6$, Figures S6–S18) and 2 ($\text{Ru}@$ $\text{Ni}_8(\text{OH})_4(\text{OH}_2)_2(\text{L2})_6$, Figures S19–S24).

Powder X-ray diffraction (PXRD) analysis showed that while the MOFs remain crystalline upon Ru incorporation (Figures S6, S14, and S19), subjecting the $\text{Ru}@$ MOF pre-

Table 1. EtOH Upgrading Results with $\text{Ru}@$ MOF Pre-catalysts in Neat EtOH Containing 21 wt% NaOEt

	variable	cat.	loading ^a	[Ru] ^b	<i>T</i> [°C]	<i>t</i> [h]	conv ^c	<i>S</i> _{total} ^d	<i>S</i> _{liq} ^e	TON ^f	TOF ^g
1	MOF support	1	0.016	2.4×10^{-7}	170	14.5	11.2	0.79	0.997	152 699	10 531
2		2	0.018	2.3×10^{-7}	170	14.5	10.7	0.74	0.997	153 471	10 584
3	maximizing TON	1	0.016	2.1×10^{-7}	170	68	26.6	0.68	0.995	414 320	6 093
4		1	0.016	9.5×10^{-8}	170	89	21.2	0.69	0.999	729 526	8 197
5	4.6 wt% NaOH	1	0.011	1.6×10^{-7}	170	14.5	6.2	0.78	0.999	123 483	8 516
6	5.7 wt% NaOEt	2	0.018	2.3×10^{-7}	170	14.5	3.9	0.99	0.999	57 660	3 976

^aRuthenium loading is expressed as a molar ratio relative to the metal in the MOF support. ^b[Ru] = moles of ruthenium used. ^cConv = conversion of EtOH. ^d*S*_{total} = overall selectivity for *n*-BuOH. ^e*S*_{liq} = selectivity for *n*-BuOH formation among liquid products. ^fTONs were calculated by dividing moles of EtOH consumed by moles of ruthenium used. ^gTOFs were calculated by dividing moles of EtOH consumed per hour by the number of moles of ruthenium. For additional information see Figures S30–S51 and Table S6.

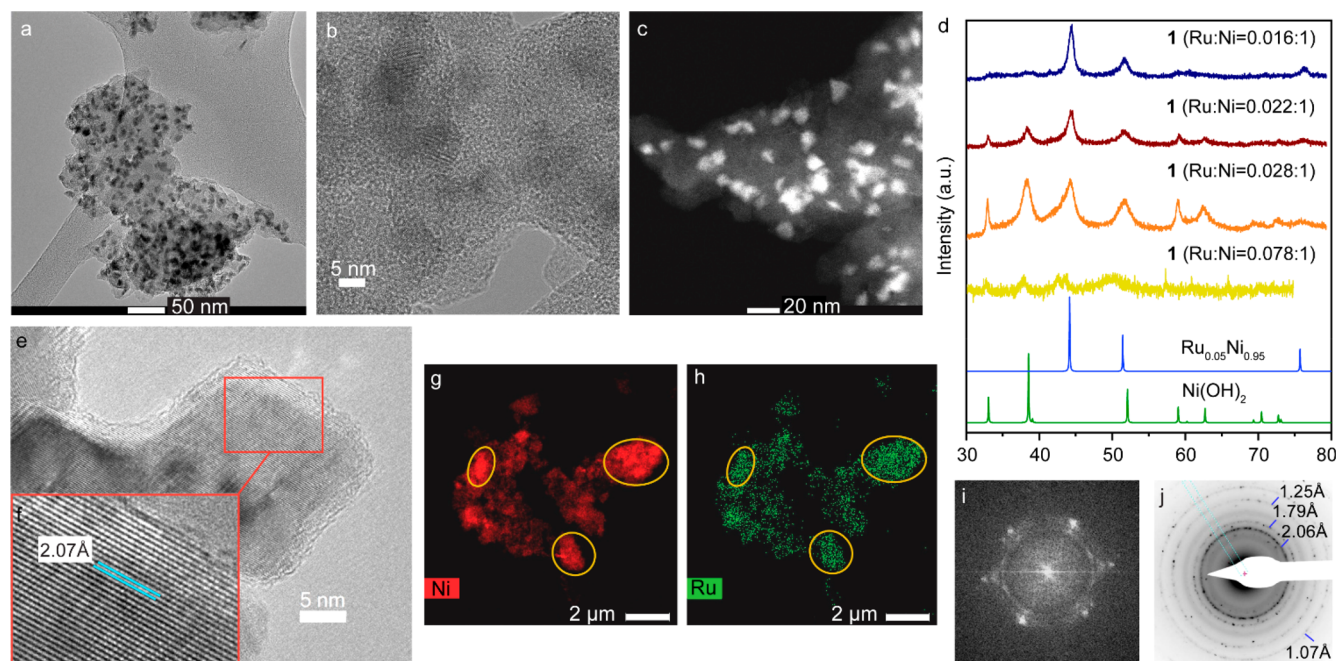


Figure 3. Characterization of recovered **1** and **2**. (a, b) TEM of **2**. (c) STEM of **2**. (d) PXRD patterns of recovered **1** with different ruthenium loadings. (e) High-resolution TEM image of recovered **1**. (f) Lattice fringes of recovered **1**. Ni (g) and Ru (h) EDS mapping for recovered **2**. (i) Fast Fourier transform of electron diffraction data from recovered **1**. (j) SAD pattern measurement of *d*-spacing for recovered **1**.

catalysts to elevated temperatures in the presence of EtOH and NaOEt led to the formation of RuNi nanoparticles (Figure S25). Importantly, formation of *n*-BuOH, the product of the Guerbet reaction of EtOH, was detected by gas chromatography–mass spectrometric (GC-MS) analysis under these reaction conditions (Figures S26–S28).

To test the premise that MOF-derived Guerbet catalysts could effectively differentiate between EtOH and *n*-BuOH as substrates for alcohol upgrading, we tested the activity of MOF-supported and unsupported ruthenium compounds toward EtOH and *n*-BuOH under otherwise identical reaction conditions. Thus, both $[\text{Ru}(\text{nbd})\text{Cl}_2]_n$ and a combination of $[\text{Ru}(\text{nbd})\text{Cl}_2]_n$ and $\text{Ni}(\text{OAc})_2$ show reasonable activity for the upgrading of both EtOH (to produce *n*-BuOH) and *n*-BuOH (to produce 2-ethyl-hexanol) (Figure 1, Table S5). In contrast, ruthenium compounds confined in the pores of MOF supports (pre-catalysts **1** and **2**) show a strong preference for EtOH as a substrate for Guerbet reactivity and exhibit negligible reactivity toward *n*-BuOH: for **2**, the site-time yield (STY) for *n*-BuOH formation exceeds the STY for 2-ethyl-hexanol by a factor of 10.5, and the selectivity for EtOH upgrading versus *n*-BuOH upgrading is further improved with **1**, which is at least 100 times more competent at forming *n*-BuOH than 2-ethyl-hexanol (Figure 1). Given that both **1** and **2** contain the same octanuclear nickel cluster, are formed from identical Ru precursors, and produce RuNi particles of similar size (average diameter 4.3 nm for **1** and 4.4 nm for **2**, see Figures S56 and S59), the large difference in substrate selectivity must be associated with the different linkers present in the MOF precursors.

Because catalyst **1** shows very low activity for the coupling of EtOH and *n*-BuOH to form C_6 alcohols 2-ethyl-butanol or 1-hexanol (Figure S29) in addition to preventing further reaction between *n*-BuOH product molecules, **1** should retain its high selectivity for *n*-BuOH formation even at high EtOH conversion.

Notably, even though previous heterogeneous Guerbet catalysts for EtOH upgrading are effective only above 200 °C, our systems exhibit high activity for EtOH upgrading as low as 170 °C, an operating temperature previously accessible only with homogeneous catalysts. Furthermore, none of the side products commonly formed with heterogeneous Guerbet catalysts (ethylene, diethyl ether, ethyl acetate, methane, or CO) are detected with our catalysts.^{6,8,11,17,18,28–30} Although NaOEt is the optimal base for promoting EtOH upgrading, it can be replaced with the more convenient NaOH with minimal loss of *n*-BuOH STY (Table 1, entry 5). Optimization of the per-ruthenium activity led to a remarkable activity of 725,000 turnovers per Ru atom after 89 h starting from **1**. This compares favorably with the current record turnover number among homogeneous catalysts, 114 120 turnovers over 168 h.²⁰

Importantly, pre-catalyst **1** leads to the production of *n*-BuOH with $99.5 \pm 0.1\%$ selectivity among liquid products at EtOH conversions up to 26.6% (Table 1, entry 3). The only products other than *n*-BuOH detected in significant quantities under these conditions are sodium acetate (NaOAc) and H_2 , common side products in Guerbet reactions (Figures S41–S44).^{16,20,22} Notably, the overall selectivity for *n*-BuOH reaches 99% (among both solid and liquid products) when the amount of NaOEt promoter is decreased (Figure 2 and Table 1, entry 6). Use of 5.7 wt% NaOEt essentially completely suppresses the formation of NaOAc and H_2 , albeit with a concomitant reduction in overall EtOH conversion to 3.9% after 14.5 h.

Because **1** and **2** can be reused without loss of activity (Figures S45 and S46), we propose that RuNi nanoparticles formed in situ and recovered after catalytic runs are the likely active catalysts. ICP-MS analysis of filtered reaction mixtures showed leaching of only 2.5% of the ruthenium content for **2**. No leaching of either nickel or ruthenium was observed for **1** after 14.5 h of catalytic operation at 170 °C (Table S7).

UV-vis analysis and hot filtration experiments showed, however, that partial leaching of entire RuNi nanoparticles occurred after prolonged reaction times (Figures S47 and S48). Analysis of the Ni 2p peaks in high-resolution XPS data indicates that a fraction of Ni^{II} is reduced to Ni⁰ under the reaction conditions (Figure S49). Microscopy and PXRD data showed that the reduced metal species form alloyed nanoparticles (Figures 3a–d and S52–S59) with an average diameter of 4.3 nm for **1** and 4.4 nm for **2**.

The only other Ni species, observed post-catalytically only in cases where a MOF precursor containing a high ruthenium loading was used, was Ni(OH)₂, which does not impact *n*-BuOH formation (Figures S50 and S51). Splitting of the diffraction peak around $2\theta = 44^\circ$ suggests that Ru as well as RuNi nanoparticles are formed at ruthenium loadings exceeding Ru:Ni = 0.028:1, likely because efficient RuNi alloy formation only occurs for low ruthenium loadings (Figure 3d). Notably, recovered catalysts containing pure Ru nanoparticles showed lower activity on a per-ruthenium basis, suggesting that optimal catalytic activity requires the formation of RuNi alloys. Analysis of the precise *d*-spacing of the PXRD peaks of RuNi nanoparticles, coupled with energy-dispersive X-ray spectroscopy (EDS) mapping (Figure 3g,h) and selected area diffraction (SAD, Figure 3j) pattern measurement of lattice fringes (Figure 3e,f) indicate that RuNi nanoparticles with a Ru content of approximately 5% (i.e., Ru_{0.05}Ni_{0.95}) are formed from **1** under the reaction conditions.³¹ Alloy formation with the SBU-derived metal partially accounts for the notable dependence of activity and selectivity on the MOF support despite the loss of crystallinity.^{32,33} The exact nature of the interaction between the MOF and the nanoparticles, as well as the possible effect of pore size, aperture, and other properties of the host MOF on catalysis are the subject of future studies.

The foregoing results show that impregnation of simple Ru precursors within a suitable MOF precursor and treatment under conditions relevant for EtOH upgrading reactions give rise to highly active catalysts that show strongly diverging activity toward two chemically similar alcohols. Pre-catalyst **1**, derived from a nickel-based MOF catalyzes EtOH upgrading with a turnover frequency of >725 000. The same pre-catalyst's very low reactivity toward *n*-BuOH ensures the stability of the desired product under the reaction conditions and leads to excellent overall selectivity for the C₄ product.

■ ASSOCIATED CONTENT

Supporting Information

The Supporting Information is available free of charge on the ACS Publications website at DOI: 10.1021/jacs.9b08968.

Experimental procedures and analytical data for all compounds, including Figures S1–S59 and Tables S1–S14 (PDF)

■ AUTHOR INFORMATION

Corresponding Author

*mdinca@mit.edu

ORCID

Mircea Dincă: 0000-0002-1262-1264

Notes

The authors declare the following competing financial interest(s): M.D. and C.N.N. are inventors on a patent application describing some of the results herein.

■ ACKNOWLEDGMENTS

This research was supported by funds from the Alan T. Waterman Award conferred by the National Science Foundation to M.D. (DMR-1645232). Fundamental studies of cation exchange in MOFs are supported through a CAREER grant to M.D. from the National Science Foundation (DMR-1452612). We thank Professor Ognjen Š. Miljanić for supplying ligand **L2** for the synthesis of Ni₈(OH)₄(OH₂)₂(**L2**)₆ and Dr. Robert Day for performing XPS analysis.

■ REFERENCES

- (1) Jenkins, A. D.; Kratochvíl, P.; Stepto, R. F. T.; Suter, U. W. Glossary of basic terms in polymer science (IUPAC Recommendations 1996). *Pure Appl. Chem.* **1996**, *68*, 2287.
- (2) Ndaba, B.; Chiyanzu, I.; Marx, S. *n*-Butanol derived from biochemical and chemical routes: A review. *Biotechnol. Rep.* **2015**, *8*, 1–9.
- (3) Szulczyk, K. Which is a better transportation fuel - Butanol or ethanol? *Int. J. Energy Environ.* **2010**, *1* (3), 501–512.
- (4) Lapuerta, M.; Ballesteros, R.; Barba, J. Strategies to Introduce *n*-Butanol in Gasoline Blends. *Sustainability* **2017**, *9* (4), 589.
- (5) Dürre, P. Fermentative Butanol Production. *Ann. N. Y. Acad. Sci.* **2008**, *1125* (1), 353–362.
- (6) Tsuchida, T.; Kubo, J.; Yoshioka, T.; Sakuma, S.; Takeguchi, T.; Ueda, W. Reaction of ethanol over hydroxyapatite affected by Ca/P ratio of catalyst. *J. Catal.* **2008**, *259* (2), 183–189.
- (7) Ogo, S.; Onda, A.; Iwasa, Y.; Hara, K.; Fukuoka, A.; Yanagisawa, K. 1-Butanol synthesis from ethanol over strontium phosphate hydroxyapatite catalysts with various Sr/P ratios. *J. Catal.* **2012**, *296*, 24–30.
- (8) Riittonen, T.; Toukonen, E.; Madnani, D. K.; Leino, A.-R.; Kordas, K.; Szabo, M.; Sapi, A.; Arve, K.; Wärnå, J.; Mikkola, J.-P. One-Pot Liquid-Phase Catalytic Conversion of Ethanol to 1-Butanol over Aluminium Oxide—The Effect of the Active Metal on the Selectivity. *Catalysts* **2012**, *2* (1), 68.
- (9) Dowson, G. R. M.; Haddow, M. F.; Lee, J.; Wingad, R. L.; Wass, D. F. Catalytic Conversion of Ethanol into an Advanced Biofuel: Unprecedented Selectivity for *n*-Butanol. *Angew. Chem., Int. Ed.* **2013**, *52* (34), 9005–9008.
- (10) Kozłowski, J. T.; Davis, R. J. Heterogeneous Catalysts for the Guerbet Coupling of Alcohols. *ACS Catal.* **2013**, *3* (7), 1588–1600.
- (11) Marcu, I.-C.; Tanchoux, N.; Fajula, F.; Tichit, D. Catalytic Conversion of Ethanol into Butanol over M–Mg–Al Mixed Oxide Catalysts (M = Pd, Ag, Mn, Fe, Cu, Sm, Yb) Obtained from LDH Precursors. *Catal. Lett.* **2013**, *143* (1), 23–30.
- (12) Chakraborty, S.; Piszal, P. E.; Hayes, C. E.; Baker, R. T.; Jones, W. D. Highly Selective Formation of *n*-Butanol from Ethanol through the Guerbet Process: A Tandem Catalytic Approach. *J. Am. Chem. Soc.* **2015**, *137* (45), 14264–14267.
- (13) Wingad, R. L.; Gates, P. J.; Street, S. T. G.; Wass, D. F. Catalytic Conversion of Ethanol to *n*-Butanol Using Ruthenium P–N Ligand Complexes. *ACS Catal.* **2015**, *5* (10), 5822–5826.
- (14) Earley, J. H.; Bourne, R. A.; Watson, M. J.; Poliakov, M. Continuous catalytic upgrading of ethanol to *n*-butanol and > C₄ products over Cu/CeO₂ catalysts in supercritical CO₂. *Green Chem.* **2015**, *17* (5), 3018–3025.
- (15) Tseng, K.-N. T.; Lin, S.; Kampf, J. W.; Szymczak, N. K. Upgrading ethanol to 1-butanol with a homogeneous air-stable ruthenium catalyst. *Chem. Commun.* **2016**, *52* (14), 2901–2904.
- (16) Xie, Y.; Ben-David, Y.; Shimon, L. J. W.; Milstein, D. Highly Efficient Process for Production of Biofuel from Ethanol Catalyzed by Ruthenium Pincer Complexes. *J. Am. Chem. Soc.* **2016**, *138* (29), 9077–9080.
- (17) Ho, C. R.; Shylesh, S.; Bell, A. T. Mechanism and Kinetics of Ethanol Coupling to Butanol over Hydroxyapatite. *ACS Catal.* **2016**, *6* (2), 939–948.

- (18) Pang, J.; Zheng, M.; He, L.; Li, L.; Pan, X.; Wang, A.; Wang, X.; Zhang, T. Upgrading ethanol to n-butanol over highly dispersed Ni–MgAlO catalysts. *J. Catal.* **2016**, *344*, 184–193.
- (19) Aitchison, H.; Wingad, R. L.; Wass, D. F. Homogeneous Ethanol to Butanol Catalysis—Guerbet Renewed. *ACS Catal.* **2016**, *6* (10), 7125–7132.
- (20) Fu, S.; Shao, Z.; Wang, Y.; Liu, Q. Manganese-Catalyzed Upgrading of Ethanol into 1-Butanol. *J. Am. Chem. Soc.* **2017**, *139* (34), 11941–11948.
- (21) Wu, X.; Fang, G.; Liang, Z.; Leng, W.; Xu, K.; Jiang, D.; Ni, J.; Li, X. Catalytic upgrading of ethanol to n-butanol over M–CeO₂/AC (M = Cu, Fe, Co, Ni and Pd) catalysts. *Catal. Commun.* **2017**, *100*, 15–18.
- (22) Kulkarni, N. V.; Brennessel, W. W.; Jones, W. D. Catalytic Upgrading of Ethanol to n-Butanol via Manganese-Mediated Guerbet Reaction. *ACS Catal.* **2018**, *8* (2), 997–1002.
- (23) Jiang, D.; Fang, G.; Tong, Y.; Wu, X.; Wang, Y.; Hong, D.; Leng, W.; Liang, Z.; Tu, P.; Liu, L.; Xu, K.; Ni, J.; Li, X. Multifunctional Pd@UiO-66 Catalysts for Continuous Catalytic Upgrading of Ethanol to n-Butanol. *ACS Catal.* **2018**, *8*, 11973–11978.
- (24) Deng, Q.; Nie, G.; Pan, L.; Zou, J.-J.; Zhang, X.; Wang, L. Highly selective self-condensation of cyclic ketones using MOF-encapsulating phosphotungstic acid for renewable high-density fuel. *Green Chem.* **2015**, *17* (8), 4473–4481.
- (25) Ahn, S.; Nauert, S. L.; Buru, C. T.; Rimoldi, M.; Choi, H.; Schweitzer, N. M.; Hupp, J. T.; Farha, O. K.; Notestein, J. M. Pushing the Limits on Metal–Organic Frameworks as a Catalyst Support: NU-1000 Supported Tungsten Catalysts for o-Xylene Isomerization and Disproportionation. *J. Am. Chem. Soc.* **2018**, *140* (27), 8535–8543.
- (26) Reiner, B. R.; Kassie, A. A.; Wade, C. R. Unveiling reactive metal sites in a Pd pincer MOF: insights into Lewis acid and pore selective catalysis. *Dalton Trans.* **2019**, *48* (26), 9588–9595.
- (27) Masciocchi, N.; Galli, S.; Colombo, V.; Maspero, A.; Palmisano, G.; Seyyedi, B.; Lamberti, C.; Bordiga, S. Cubic Octanuclear Ni(II) Clusters in Highly Porous Polypyrazolyl-Based Materials. *J. Am. Chem. Soc.* **2010**, *132* (23), 7902–7904.
- (28) Onyestyák, G.; Novodárszki, G.; Wellisch, Á. F.; Valyon, J.; Thakur, A. J.; Deka, D. Guerbet self-coupling for ethanol valorization over activated carbon supported catalysts. *React. Kinet., Mech. Catal.* **2017**, *121* (1), 31–41.
- (29) León, M.; Díaz, E.; Vega, A.; Ordóñez, S.; Auroux, A. Consequences of the iron–aluminium exchange on the performance of hydrotalcite-derived mixed oxides for ethanol condensation. *Appl. Catal., B* **2011**, *102* (3), 590–599.
- (30) Kozłowski, J. T.; Behrens, M.; Schlögl, R.; Davis, R. J. Influence of the Precipitation Method on Acid–Base-Catalyzed Reactions over Mg–Zr Mixed Oxides. *ChemCatChem* **2013**, *5* (7), 1989–1997.
- (31) Raub, E.; Menzel, D. Die Nickel-Ruthenium-Legierung. *Z. Metallkd.* **1961**, *52* (12), 831–833.
- (32) Mori, K.; Miyawaki, K.; Yamashita, H. Ru and Ru–Ni Nanoparticles on TiO₂ Support as Extremely Active Catalysts for Hydrogen Production from Ammonia–Borane. *ACS Catal.* **2016**, *6* (5), 3128–3135.
- (33) Roy, S.; Pachfule, P.; Xu, Q. High Catalytic Performance of MIL-101-Immobilized NiRu Alloy Nanoparticles towards the Hydrolytic Dehydrogenation of Ammonia Borane. *Eur. J. Inorg. Chem.* **2016**, *2016* (27), 4353–4357.